POLITECNICO DI TORINO
Repository ISTITUZIONALE

Frequency Coordinated Control for the Asynchronous Interconnected Power System With Multiple HVDC Links

(Article begins on next page)

14 May 2024

RESEARCH ARTICLE

Frequency Coordinated Control for the Asynchronous Interconnected Power System With Multiple HVDC Links

YI HU [1], **XIA LEI** [1], **(Member, IEEE), TAO HUANG** [2], **(Member, IEEE), AND YU ZHANG** [3]

[1] School of Electrical Engineering and Electronic Information, Xihua University, Chengdu 610039, China
[2] Department of Energy, Polytechnic University of Turin, 10129 Turin, Italy
[3] School of Electrical Engineering, Southwest Jiaotong University, Chengdu 611756, China

Corresponding authors: Yi Hu (huangganghuyi@163.com) and Xia Lei (snow_lei246@mail.xhu.edu.cn)

ABSTRACT The isolation of the HVDC transmission system challenges the frequency stability of asynchronous power grid. Considering the high-capacity power regulation capability of multiple HVDC links, a novel frequency coordinated control method is proposed for the asynchronous interconnected power system. This method firstly establishes a detailed frequency response analysis model by using wide-area measurement data. Then, for the lowest frequency control after disturbance, based on the frequency response analysis model, the functional relationship between the lowest frequency and DC power support is deduced. Finally, considering the influence of multiple HVDC power support on node voltage, power flow of line and frequency variation of the HVDC opposite-end grids, an optimal model of frequency coordination control with minimal influence is established. By solving the model, an multiple HVDC coordinated power support scheme can be obtained to achieve the lowest frequency control target after disturbance. A typical IEEE system is improved to an asynchronous interconnected power grid for case simulation. The accuracy and effectiveness of the proposed frequency coordination control are verified by comparison with traditional method.

INDEX TERMS Asynchronous interconnected, power system, DC power support, multiple HVDC, frequency analysis, frequency coordinated control.

I. INTRODUCTION

High Voltage Direct Current (HVDC) transmission system has the advantages of lower investment costs, lower losses, and environmental benefits. It has been extensively used in long-distance and large capacity power transmission [1], [2], [3]. Asynchronous grids interconnection is one of the important applications of HVDC. With the increase in such asynchronous interconnection projects, the asynchronous interconnected power grid with multiple HVDC has emerged, as shown in Fig. 1. For example, the three regional grids in North America, the Eastern Interconnection, Western Interconnection and ERCOT Interconnection currently operate

The associate editor coordinating the review of this manuscript and approving it for publication was Huiyan Zhang.

asynchronously through HVDC [4]; The Yunnan Provincial Power Grid in Southwest China and several other surrounding provincial power grids have realized the internal asynchronous interconnection of the Southern Power Grid through multiple HVDC [5]. The asynchronous interconnection makes the large power grid gradually divided into multiple independent sub-grids, which weakens the inertia of the power grid and reduces the frequency mutual support between AC grids. When a large disturbance occurs, the frequency stability problem of the aforementioned power grid would be more serious due to low inertia, which deserves our attention.

From the major blackout occurred in nearly years, it can be seen that when the power grid is greatly disturbed, and no effective control measures are taken, the grid frequency will
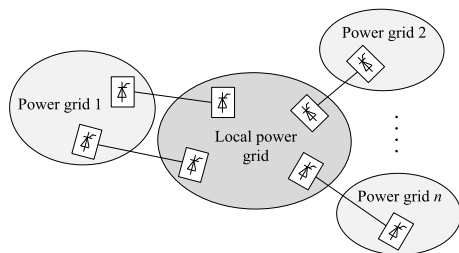
FIGURE 1. The multiple HVDC asynchronous system.

be greatly offset and the event of frequency collapse may be caused [6]. Although traditional under-frequency load shedding has a certain effect on preventing frequency collapse, it is limited in capacity and slow in response [7]. In order to make up for the shortcomings of traditional control, some more accurate and faster load shedding studies have been carried out [8], [9], [10], [11]. However, excessive load shedding does not meet the economic operation requirements of the power grid. Considering the HVDC has strong controllability and rapid adjustment capability for its transmission power, it can be used for emergency DC power support (EDCPS) [12], [13], [14], [15]. Therefore, how to make full use of the multiple HVDC EDCPS to ensure the frequency security of asynchronous power grid is of great significance.

Some studies have done relevant work on this aspect. In [16] and [17], a frequency coordinated control method for MT-HVDC grids with wind power plants is proposed. This method uses the power of offshore WPPs to contribute to the primary frequency control of the land asynchronous AC grids. In addition, a novel primary frequency control of interconnected time-delay power systems is proposed in [18], which relies on the design of the robust distributed HVDC controllers. In [19], the authors propose a frequency control strategy for voltage source converter based VSC-MTDC to facilitate the exchange of primary frequency reserves among asynchronous AC grids, thus providing frequency support from each others. For the asynchronous interconnected Yunnan power grid in China, [20] studies the frequency characteristics under various control schemes, and analyzes that the frequency coordinated control can be realized by reasonably setting the controller parameters. In [21], an adaptive droop control strategy for multi-terminal HVDC network is proposed to provide frequency support and power sharing via a distributed consensus algorithm. Similarly, [22] has designed a coordinated droop control mechanism among LCC-HVDC systems and generators.

The above existing researches are mainly through the design of coordinated controller to achieve multiple HVDC participation frequency control, and the most critical is the controller parameter setting [23]. However, the existing researches are usually set by human experience or obtained by fitting the frequency response curve of specific power grid and specific disturbance [24], [25] This makes the adaptive ability of the controller weak and the portability poor.

More importantly, these methods can not consider the adverse effects of multiple HVDC control schemes on node voltage, power flow of line and frequency variation of interconnected power grids. In view of the above problems, this paper avoids the idea of complex controller design and control parameter tuning, and carries out a new frequency coordinated control research from the mathematical relationship among the power grid disturbance, the frequency control target and the multi-HVDC EDCPS.

Considering that the lowest frequency after disturbance is the most concerned frequency characteristic of power grid operators, and the low value of the lowest frequency is an important reason to induce cascading faults and frequency accidents. Therefore, this paper proposes a multi-HVDC coordinated control method for the lowest frequency safety by using multi-HVDC EDCPS. When a power disturbance is detected in the power grid,, this method first quickly predicts the frequency dynamic response after disturbance. If the lowest frequency exceeds the security level, the method will use a coordinated control optimization model to calculate the optimal EDCPS of each HVDC line. The proposed frequency coordinated control mainly has the following contributions and advantages:

- A detailed frequency response analysis model is established, which is different from the traditional equivalent model. The model includes the motion equation of all generators, primary frequency control equation, governor characteristics, network loss, frequency variation effect of load and DC power variation. This model can more truly reflect the frequency response characteristics after disturbance.

- The control strategy obtained by the established optimization model can not only restore the lowest frequency after the power grid disturbance to the target safety level, but also ensure that the node voltage of the power grid, the power flow of the lines and the frequency variation of all the opposite-end power grids remain in a safe state after the control is implemented.

The remainder of this paper is organized as follows. Section II and Section III introduce the construction process of frequency response analysis model. The coordinated control optimization model and its solution method are introduced in Section IV. In Section V, the effectiveness of the proposed method is verified by using the modified IEEE 50-generator system. Finally, the conclusions of the case study are given in Section VI.

II. SYSTEM MODELLING

According to the definition of center-of-inertia (COI) [26], the increment equation of system average frequency is defined as:

$$\Delta\omega_s = \sum_{i=1}^{n}(H_i\Delta\omega_i)/\sum_{i=1}^{n}H_i \tag{1}$$

where H_i is inertial time constant; ω_i is the angular frequency of the generator; n is the number of the generators.

A. POWER SYSTEM NETWORK EQUATIONS

For each node in the power grid, the injected active power P_i and reactive power P_i can be formulated as:

$$P_i = V_i \sum_{j=1}^{n+m} V_j(G_{ij} \cos \theta_{ij} + B_{ij} \sin \theta_{ij}) \tag{2}$$

$$Q_i = V_i \sum_{j=1}^{n+m} V_j(G_{ij} \sin \theta_{ij} - B_{ij} \cos \theta_{ij}) \tag{3}$$

where V_i, V_j are the voltages of nodes i and j; G_{ij}, B_{ij} are conductance and susceptance, respectively; θ_{ij} is the voltage phase difference of nodes i and j.

According to the Newton-Raphson method, the power increment equations can be obtained by linearizing (2) and (3):

$$\begin{bmatrix} \Delta \boldsymbol{P}_G \\ \Delta \boldsymbol{P}_L \\ \Delta \boldsymbol{Q}_L \end{bmatrix} = - \begin{bmatrix} \boldsymbol{H}_{GG} & \boldsymbol{H}_{GL} & \boldsymbol{N}_G \\ \boldsymbol{H}_{LG} & \boldsymbol{H}_{LL} & \boldsymbol{N}_L \\ \boldsymbol{J}_{LG} & \boldsymbol{J}_{LL} & \boldsymbol{L}_L \end{bmatrix} \begin{bmatrix} \Delta \boldsymbol{\theta}_G \\ \Delta \boldsymbol{\theta}_L \\ \Delta \boldsymbol{V}_L / \boldsymbol{V}_{L0^+} \end{bmatrix} \tag{4}$$

where $\Delta \boldsymbol{P}_G$ represents electromagnetic power increment of generator node; $\Delta \boldsymbol{P}_L$, $\Delta \boldsymbol{Q}_L$ represent the active and reactive power increments of load nodes respectively; $\Delta \boldsymbol{\theta}_G$, $\Delta \boldsymbol{\theta}_L$ are variation of node voltage phase angle; $\Delta \boldsymbol{V}_L$ is variation of voltage amplitude.

B. GENERATOR POWER INCREMENTAL EQUATIONS

Taking the power angle of the generator k as the reference, the rotor motion equation of generator i is:

$$\begin{cases} \dfrac{d \Delta \delta_i}{dt} = (\Delta \omega_i - \Delta \omega_k) \omega_B \\ M_i \dfrac{d \Delta \omega_i}{dt} = \Delta P_{mi} - \Delta P_{ei} + (P_{mi0^+} - P_{ei0^+}) \end{cases} \tag{5}$$

where subscript 0^+ represents the instant after disturbance; δ_i is the generator power angle; ω_B is the system reference frequency; ΔP_{mi}, ΔP_{ei} are the mechanical and electromagnetic power increment of generator; M_i is the inertia constant of generator.

The governor system of the turbine is closely related to the frequency dynamic process, so in this section, the linearized turbine-governor model is considered as:

$$\begin{bmatrix} \Delta \dot{P}_{Ti} \\ \Delta \dot{v}_i \end{bmatrix} = \begin{bmatrix} -\dfrac{1}{T_{3i}} & \dfrac{T_{1i}-T_{2i}}{T_{1i}T_{3i}} \\ 0 & -\dfrac{1}{T_{1i}} \end{bmatrix} \begin{bmatrix} \Delta P_{Ti} \\ \Delta v_i \end{bmatrix} - \begin{bmatrix} \dfrac{T_{2i}}{R_i T_{1i} T_{3i}} \\ \dfrac{1}{R_i T_{1i}} \end{bmatrix} \Delta \omega_i \tag{6}$$

$$\Delta P_{mi} = \begin{bmatrix} 1 & 0 \end{bmatrix} \begin{bmatrix} \Delta P_{Ti} \\ \Delta v_i \end{bmatrix} - D_{ti} \Delta \omega_i \tag{7}$$

where ΔP_{Ti}, Δv_i are power and valve opening increment of the turbine; T_{1i}, T_{2i}, T_{3i} are time constants of the turbine-governor; R_i, D_{ti} are adjustment coefficient and damping coefficient of the turbine-governor.

C. LOAD POWER INCREMENTAL EQUATIONS

Considering the frequency variation and voltage variation effects of load, the power incremental equation of load node
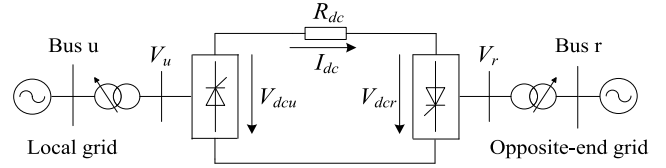

FIGURE 2. The structure diagram of HVDC interconnected power grid.

can be linearly described as

$$\begin{cases} \Delta P_{Li} = -\dfrac{\partial P_{Li}}{\partial \omega_s} \Big|_{0^+} \Delta \omega_s - \dfrac{\partial P_{Li}}{\partial V_{Li}/V_{Li}} \Big|_{0^+} \dfrac{\Delta V_{Li}}{V_{Li}} \\ \Delta Q_{Li} = -\dfrac{\partial Q_{Li}}{\partial \omega_s} \Big|_{0^+} \Delta \omega_s - \dfrac{\partial Q_{Li}}{\partial V_{Li}/V_{Li}} \Big|_{0^+} \dfrac{\Delta V_{Li}}{V_{Li}} \end{cases} \tag{8}$$

D. DC POWER INCREMENTAL EQUATIONS

This paper takes the sending-out HVDC as an example to deduce the power equations of DC node. Fig. 2 is the schematic diagram of HVDC link.

For the sending-end converter of HVDC, the quasi-steady model is:

$$\begin{cases} V_{dcu} = V_{d0} \cos \alpha - (3X_c/\pi) I_{dc} \\ P_{dc} = V_{dcu} I_{dc} \\ Q_{dc} = P_{dc} \tan \varphi \\ V_{d0} = (3\sqrt{2}/\pi) V_u \\ \cos \varphi = V_{dcu}/V_{d0} \end{cases} \tag{9}$$

where V_{d0} is the ideal DC voltage; V_u is the AC voltage at the converter side; α is the trigger angle of converter; I_{dc}, V_{dcu} are the DC current and DC voltage respectively; X_c is the equivalent reactance; P_{dc}, Q_{dc} are the active power and reactive power absorbed by the converter; φ is the power factor angle.

In order to formulate the power equations of DC nodes more conveniently, constant DC current control and constant DC voltage control are adopted in the rectifier and inverter respectively. Considering the equivalent loss resistance R_{dc} of the DC line, the rectifier-side DC voltage V_{dcu} can be stated as:

$$V_{dcu} = R_{dc} I_{dc} + V_{dcr} \tag{10}$$

The nonlinear coupling relationship between P_{dc} and Q_{dc} of the sending-end converter can be derived from (9) and (10).

$$\begin{cases} Q_{dc} = P_{dc} \sqrt{\dfrac{18 V_u^2}{V_{dcu}^2 \pi^2} - 1} \\ V_{dcu} = \dfrac{V_{dcr} + \sqrt{V_{dcr}^2 + 4R_{dc}P_{dc}}}{2} \end{cases} \tag{11}$$

Since the active power and reactive power of the DC node are usually known, it can be considered that its characteristics are similar to those of the load node. Assuming that the EDCPS is ΔP_{dcCi}, the DC node power incremental equations

after linearization can be calculated as:

$$
\begin{cases}
\Delta P_{Ldci} = \Delta P_{Li} + \Delta P_{dci} \\
\qquad = -\frac{\partial P_{Li}}{\partial \omega_s}\big|_{0^+}\Delta\omega_s - \frac{\partial P_{Li}}{\partial V_{Li}/V_{Li}}\big|_{0^+}\frac{\Delta V_{Li}}{V_{Li}} + \Delta P_{dci} \\
\Delta Q_{Ldci} = \Delta Q_{Li} + \Delta Q_{dci} \\
\qquad = -\frac{\partial Q_{Li}}{\partial \omega_s}\big|_{0^+}\Delta\omega_s - \frac{\partial Q_{Li}}{\partial V_{Li}/V_{Li}}\big|_{0^+}\frac{\Delta V_{Li}}{V_{Li}} + \Delta Q_{dci}
\end{cases}
\tag{12}
$$

where ΔP_{Ldci}, ΔQ_{Ldci} are DC node power increments respectively

III. ANALYSIS MODEL OF FREQUENCY DYNAMIC

Assuming that all node frequencies are approximated to the system average frequency, and substituting (8) and (12) into (4), then we can get:

$$
\begin{bmatrix} \Delta P_G \\ 0 \\ 0 \end{bmatrix} = -\begin{bmatrix} H_{GG} & H_{GL} & N_G & E \\ H_{LG} & H_{LL} & N'_L & F \\ J_{LG} & J_{LL} & L'_L & S \end{bmatrix}\begin{bmatrix} \Delta\theta_G \\ \Delta\theta_L \\ \Delta V_L/V_{L0^+} \\ \Delta\omega_s \end{bmatrix}
$$
$$
-\begin{bmatrix} 0 \\ \Delta P_{dc} \\ \Delta Q_{dc} \end{bmatrix}
\tag{13}
$$

where $E = 0$, it is an n-dimensional column vector; $F = \partial P_L/\partial\omega_s$; $N'_L = N_L - \frac{\partial P_L}{\partial V_L/V_L}$; $L'_L = L_L - \frac{\partial Q_L}{\partial V_L/V_L}$.

By eliminating $\Delta\theta_L$ and $\Delta V_L/V_{L0^+}$, Eq. (13) can be expressed as the electromagnetic power increment equation of generator nodes.

$$
\Delta P_G = -\begin{bmatrix} H_N & E_N & F_N & S_N \end{bmatrix}\begin{bmatrix} \Delta\theta_G \\ \Delta P_{dc} \\ \Delta Q_{dc} \\ \Delta\omega_s \end{bmatrix}
\tag{14}
$$

where

$$
H_N = (H_{GG} - H_{GL}H_{LL}^{-1}H_{LG}) - (N_G - H_{GL}H_{LL}^{-1}N'_L)
$$
$$
\times(L'_L - J_{LL}H_{LL}^{-1}N'_L)\times(J_{LG} - J_{LL}H_{LL}^{-1}H_{LG});
$$
$$
E_N = -H_{GL}H_{LL}^{-1} + J_{LL}H_{LL}^{-1}\times(N_G - H_{GL}H_{LL}^{-1}N'_L)
$$
$$
\times(L'_L - J_{LL}H_{LL}^{-1}N'_L)^{-1};
$$
$$
F_N = (H_{GL}H_{LL}^{-1}N'_L - N_G)\times(L'_L - J_{LL}H_{LL}^{-1}N'_L)^{-1};
$$
$$
S_N = (E - H_{GL}H_{LL}^{-1}F) - (N_G - H_{GL}H_{LL}^{-1}N'_L)\times(L'_L
$$
$$
-J_{LL}H_{LL}^{-1}N'_L)^{-1}\times(S - J_{LL}H_{LL}^{-1}F).
$$

By substituting (7) and (14) into (5), and then combining with (6), the frequency response analysis model of the multiple HVDC asynchronous system can be obtained as:

$$
\begin{cases}
\begin{bmatrix} \Delta\dot\theta_G \\ \Delta\dot\omega \\ \Delta\dot P_{Ti} \\ \Delta\dot v_i \end{bmatrix} = \begin{bmatrix} 0 & K_{12} & 0 & 0 \\ K_{21} & K_{22} & K_{23} & 0 \\ 0 & K_{32} & K_{33} & K_{34} \\ 0 & K_{42} & 0 & K_{44} \end{bmatrix}\begin{bmatrix} \Delta\theta_G \\ \Delta\omega \\ \Delta P_{Ti} \\ \Delta v_i \end{bmatrix} + \begin{bmatrix} 0 \\ K_5 \\ 0 \\ 0 \end{bmatrix} \\
\Delta\omega_s = \begin{bmatrix} 0 & K_6 & 0 & 0 \end{bmatrix}\begin{bmatrix} \Delta\theta_G \\ \Delta\omega \\ \Delta P_{Ti} \\ \Delta v_i \end{bmatrix}
\end{cases}
\tag{15}
$$

where the coefficient matrix K_{12}, K_{21}, K_{22}, K_{23}, K_{32}, K_{33}, K_{34}, K_{42}, K_{44}, K_5 and K_6 are calculated as:

$$
K_{12} = \begin{bmatrix} & & & k-\text{th column} & & & \\ 1 & & & -1 & & & \\ & \ddots & & \vdots & & 0 & \\ & & 1 & -1 & & & \\ & & & -1 & 1 & & \\ & 0 & & \vdots & & \ddots & \\ & & & -1 & & & 1 \end{bmatrix}\omega_B
$$

$$
K_{21} = \mathrm{diag}\{1/M_i\}\times H_N
$$
$$
K_{22} = S_N\times\begin{bmatrix} M_1 & \cdots & M_m \end{bmatrix}/M_T + \mathrm{diag}\{-D_{ti}/M_i\}
$$
$$
K_{23} = \mathrm{diag}\{1/M_i\}
$$
$$
K_{32} = \mathrm{diag}\{-T_{2i}/(R_iT_{1i}T_{3i})\}
$$
$$
K_{33} = \mathrm{diag}\{-1/T_{3i}\}
$$
$$
K_{34} = \mathrm{diag}\{(T_{1i} - T_{2i})/(T_{1i}T_{3i})\}
$$
$$
K_{42} = \mathrm{diag}\{-1/(R_iT_{1i})\}
$$
$$
K_{44} = \mathrm{diag}\{-1/T_{1i}\}
$$
$$
K_5 = \mathrm{diag}\{1/M_i\}\times\left\{\begin{bmatrix} P_{m10^+}-P_{e10^+} & \cdots & P_{mn0^+}-P_{en0^+} \end{bmatrix}^T\right.
$$
$$
\left. + (E_N\times\Delta P_{dc} + F_N\times\Delta Q_{dc})\right\}
$$
$$
K_6 = \begin{bmatrix} M_1 & \cdots & M_n \end{bmatrix}/M_T
$$

Eq. (15) can be expressed as the following state equation:

$$
\begin{cases}
\dot x(t) = Ax(t) + b \\
\Delta\omega_s(t) = cx(t)
\end{cases}
\tag{16}
$$

where A, b, c indicate the state matrix, input matrix and output matrix respectively; $x(t)$ is the state variable.

Using the linear system theory to solve the state equation, the frequency dynamic can be calculated:

$$
\Delta\omega_s(t) = c\sum_{i=1}^r(u_iw_i)\left[X_0e^{\lambda_it} + b\int_0^t e^{\lambda_i(t-\tau)}\mathrm{d}\tau\right]
$$
$$
= c\sum_{i=1}^r\frac{(u_iw_i)b(1-e^{\lambda_it})}{-\lambda_i}
\tag{17}
$$

where r represent the order of the state equation; λ_i represent the i-th eigenvalue of the state matrix; u_i is the right eigenvector corresponding to the i-th eigenvalue; w_i is the i-th row of the matrix after inversion of the right feature matrix; X_0 is the initial state of the state equation, and its elements are all 0.

Therefore, when the disturbance is occurred in the power grid, the data such as P_{ei0^-}, P_{ei0^+}, P_{Li0^+}, Q_{Li0^+}, V_{i0^+}, θ_{i0^+}, ω_{s0^+} and so on can be obtained by WAMS at the time of 0^+ firstly; And then taking into account ΔP_{dci} of each HVDC link; Finally, using the frequency analysis model in (17), the lowest value of the post-disturbance frequency will be predicted.

IV. FREQUENCY COORDINATED CONTROL WITH MULTIPLE HVDC LINKS

When the lowest prediction frequency ω_{smin} exceeds the frequency security range level ω_{Lmin}, the proposed method will start the coordinated control and use the multi-HVDC EDCPS to restore frequency security.

The different apportionment of EDCPS will have different effects on the local and interconnected power grids. Therefore, in order to take into account the security and stability requirements of the power grids after the control implemented, It is indispensable to formulate an optimization model to obtain the most reasonable EDCPS apportionment.

A. OBJECTIVE FUNCTION

Considering that different EDCPS apportionment will also affect the frequency variation of the opposite-end power grids differently, the minimum frequency variation of the HVDC opposite-end grids is preferred as the objective function of the optimization model to be established:

$$\min f(\Delta P_{dci}) = \sum_{i=1}^{m_1} |\Delta\omega_{sIi}| \tag{18}$$

where m_1 is the number of HVDC links, $\Delta\omega_{sIi}$ is the frequency variation of the HVDC opposite-end grid.

B. EQUALITY CONSTRAINT

Assuming that ω_{set} is the lowest value of the post-disturbance frequency, then $\omega_{set} = \omega_{smin}$ should be satisfied. When the lowest value is below the security level, there will be:

$$\Delta\omega_{smin} = \omega_{set} - \omega_{s0+} \tag{19}$$

Therefore, according to the frequency analysis model of the post-disturbance frequency, the primary equality constraint can be obtained:

$$\omega_{set} - \omega_{s0+} = c\sum_{i=1}^{r} \frac{(u_i w_i)b(1 - e^{\lambda_i t_{min}})}{-\lambda_i} \tag{20}$$

Considering that the lowest frequency value appears at the stationary point of the frequency dynamic curve, so the second equality constraint is:

$$c\sum_{i=1}^{r} \left[(u_i w_i)b e^{\lambda_i t_{min}} \right] = 0 \tag{21}$$

For each HVDC link, the active power and reactive power should always satisfy the coupling relationship, so the third equality constraint can be obtained according to (8).

$$\begin{cases} (Q_{dcj0+} + \Delta Q_{dcj}) = (P_{dci0+} + \Delta P_{dci})\sqrt{\frac{18V_{ui}^2}{V_{dcui}^2 \pi^2} - 1} \\ V_{dcui} = \dfrac{V_{dcri} + \sqrt{V_{dcri}^2 + 4R_{dci}(P_{dci0+} + \Delta P_{dci})}}{2} \end{cases} \tag{22}$$

C. INEQUALITY CONSTRAINTS

Since the post-disturbance frequency dynamic curve will have more than one stagnation point, new constraints need to be added in order to distinguish the only lowest point. Considering that the time parameter t_{min} in (20) and (21) should only correspond to the lowest frequency point, so the new constraint should be formulated as the convexity and concavity of the curves before and after this point. Therefore, when the tiny time window $(t_{min} - t_{tiny}, t_{min})$ and $(t_{min}, t_{min} + t_{tiny})$ are chosen before and after t_{min}, the first inequality constraints can be expressed as:

$$\begin{cases} t_{min} < t_{Fmin} \\ c\sum_{i=1}^{r} \left[(u_i w_i)b e^{\lambda_i(t_{min} - t_{tiny})} \right] < 0 \\ c\sum_{i=1}^{r} \left[(u_i w_i)b e^{\lambda_i(t_{min} + t_{tiny})} \right] > 0 \end{cases} \tag{23}$$

where t_{Fmin} is the time corresponding to lowest point of the frequency dynamic curve.

For the HVDC transmission system, the overload capacity of the transmission power is limited. So the EDCPS of each HVDC link should meet the second inequality constraint:

$$\Delta P_{dcmini} \leq \Delta P_{dci} \leq \Delta P_{dcmaxi} \tag{24}$$

where ΔP_{dcmini} and ΔP_{dcmaxi} are respectively the active power support limits.

The different multi-HVDC EDCPS will have different power flow changes for the grid. If the apportionment is unreasonable, it is likely that some AC lines will be overloaded and some node voltages will exceed the security range after the frequency control is implemented. This requires that the proposed control not only need to achieve the frequency control goal, but also ensure the power flow and the nodes voltage within the security range.

If (V_{Lmin}, V_{Lmax}) is defined as voltage security range, the post-disturbance node voltage should satisfy:

$$V_{Lmin} \leq V_{L\infty} \leq V_{Lmax} \tag{25}$$

where subscript ∞ represents the steady-state after disturbance.

Generally, the electromagnetic power increment of the generator can be described as:

$$\Delta P_{ei} = \Delta P_{mi} - \Delta P_{ai} \tag{26}$$

where ΔP_{ai} is the acceleration power of generator.

Considering the instantaneous moment and the steady-state after disturbance, there are:

$$\Delta P_{mi} = P_{mi\infty} - P_{mi0+} = -K_{Gi}\Delta\omega_{\infty} \tag{27}$$

$$\Delta P_{ai} = P_{ai\infty} - P_{ai0+} = -P_{ai0+} \tag{28}$$

where K_{Gi} is the frequency adjustment coefficient of generator.

Substituting (27) and (28) into (26), there will be:

$$\Delta P_{ei} = -K_{Gi}\Delta\omega_{\infty} + P_{ai0+} \tag{29}$$

And then (30) can be derived from (29) and (13) as:

$$
B = -A \begin{bmatrix} \Delta\theta_{G\infty} \\ \Delta\theta_{L\infty} \\ \Delta V_{L\infty}/V_{L0+} \\ \Delta\omega_{s\infty} \end{bmatrix} - \begin{bmatrix} 0 \\ \Delta P_{dc} \\ \Delta Q_{dc} \end{bmatrix} \quad (30)
$$

where

$$
A = \begin{bmatrix} H_{GG} & H_{GL} & N_G & -K_G \\ H_{LG} & H_{LL} & N'_L & F \\ J_{LG} & J_{LL} & L'_L & S \end{bmatrix}; B = \begin{bmatrix} P_{a0+} & 0 & 0 \end{bmatrix}^T.
$$

Assuming that the number of generator nodes and load nodes (including DC nodes) are n and m respectively, then the voltage of load nodes and the phase angle of all nodes can be calculated as:

$$
\begin{cases} \Delta V_{L\infty}/V_{L0+} = S_1 B - S_1 \begin{bmatrix} 0 & \Delta P_{dc} & \Delta Q_{dc} \end{bmatrix}^T \\ \Delta\theta_\infty = S_2 B - S_2 \begin{bmatrix} 0 & \Delta P_{dc} & \Delta Q_{dc} \end{bmatrix}^T \end{cases} \quad (31)
$$

where S_1 represents the matrix composed of the $(n+m-1)$-th row to the $(n+2m-2)$-th row of A^{-1}; S_2 represents the matrix composed of the 1-th row to the $(n+m-2)$-th row of A^{-1}.

Considering the security requirements of the node voltage, the third inequality constraint below can be obtained from (31).

$$
\begin{cases} V_{Lmin} \leq V_{L0+} + \Delta V_{L\infty} \leq V_{Lmax} \\ \Delta V_{L\infty}/V_{L0+} = S_1 B - S_1 \begin{bmatrix} 0 & \Delta P_{dc} & \Delta Q_{dc} \end{bmatrix}^T \end{cases} \quad (32)
$$

By deriving the power flow equation of the grid, the transmission power of line ij can be obtained:

$$
P_{Tij} = V_i^2(G_{ii} + G_{ij}) - V_i V_j(G_{ij}\cos\theta_{ij} + B_{ij}\sin\theta_{ij}) \quad (33)
$$

Assuming that the line transmission power limit is P_{Tmax}, the fourth inequality constraint can be formulated as:

$$
\begin{cases} V_{Li\infty} = V_{Li0+} + \Delta V_{Li\infty} \\ \Delta V_{Li\infty}/V_{Li0+} = S_{1i} B - S_{1i} \begin{bmatrix} 0 & \Delta P_{dc} & \Delta Q_{dc} \end{bmatrix}^T \\ \theta_{i\infty} = \theta_{i0+} + \Delta\theta_{i\infty} \\ \Delta\theta_{i\infty} = S_{2i} B - S_{2i} \begin{bmatrix} 0 & \Delta P_{dc} & \Delta Q_{dc} \end{bmatrix}^T \\ V_{Li\infty}^2(G_{ii} + G_{ij}) - V_{Li\infty} V_{Lj\infty}(G_{ij}\cos\theta_{ij\infty} \\ + B_{ij}\sin\theta_{ij\infty}) < P_{Tmaxij} \end{cases} \quad (34)
$$

where S_{1i}, S_{2i} are the i-th row of S_1 and S_2 respectively.

With the change of multiple HVDC transmission power, the power imbalance will appear in opposite-end grids, resulting in frequency fluctuations. At this time, the opposite-end grids frequency deviation may exceed the frequency security range. Therefore, the optimization model should also consider the opposite-end grids frequency deviation to meet the safety requirements after the control is implemented.

For the interconnected power grids, it can be formulated by the single-generator equivalent model shown in (35).

$$
\begin{cases} H_\Sigma \dfrac{d\omega_{sI}}{dt} = \sum_{i=1}^n P_{mi} - \sum_{i=1}^n P_{ei} = P_{aI} \\ \dfrac{d\theta_{sI}}{dt} = \omega_{sI} \end{cases} \quad (35)
$$

where ω_{sI}, θ_{sI}, P_{aI} are the average frequency, the generator phase angle and acceleration power of the interconnected power grid; $H_\Sigma = \sum_{i=1}^n H_i$.

If ΔP_{dcr} is defined as the EDCPS of HVDC receiving-end, then P_{aI} can be expressed as:

$$
P_{aI} = P_{aI0} - \Delta P_{aI} = \Delta P_{dcr} - D_I \Delta\omega_{sI} \quad (36)
$$

where D_I is the frequency adjustment coefficient.

From (35) and (36), the equation in (37) can be obtained:

$$
H_\Sigma \frac{d\omega_{sI}}{dt} = \Delta P_{dcr} - D_I(\omega_{sI} - \omega_{sI0+}) \quad (37)
$$

By solving (37), the opposite-end grid frequency is calculated as:

$$
\omega_{sI} = \omega_{sI0+} + \Delta P_{dcr}/D_I \quad (38)
$$

Considering the HVDC line loss, the DC power of the sending-end ΔP_{dc} and opposite-end ΔP_{dcr} should satisfy:

$$
\begin{cases} \Delta P_{dcr} = \Delta P_{dc} - \dfrac{(V_{dcu} - V_{dcr})^2}{R_{dc}} \\ V_{dcu} = \dfrac{V_{dcr} + \sqrt{V_{dcr}^2 + 4R_{dc}(P_{dc0+} + \Delta P_{dc})}}{2} \end{cases} \quad (39)
$$

Setting the security range of the steady-state frequency is $(\omega_{sImini}, \omega_{sImaxi})$, then the last inequality constraint for each HVDC link can be obtained:

$$
\begin{cases} \omega_{sImini} \leq \omega_{sI_{i0+}} + \Delta\omega_{sIi} \leq \omega_{sImaxi} \\ \Delta\omega_{sIi} = [\Delta P_{dci} - \dfrac{(V_{dcui} - V_{dcri})^2}{R_{dci}}]/D_{Ii} \\ V_{dcui} = \dfrac{V_{dcri} + \sqrt{V_{dcri}^2 + 4R_{dci}(P_{dci0+} + \Delta P_{dci})}}{2} \end{cases} \quad (40)
$$

D. OPTIMIZATION ALGORITHM

Summarizing the aforementioned analysis, the optimization model for frequency coordinated control of the asynchronous power system with multiple HVDC can be formulated: the objective function has been presented in (18); the equality constraints are shown in (20), (21) and (22); the inequality constraints are shown in (23), (24), (32), (34) and (40).

There are many methods to solve the above optimization problems [27], [28]. Considering the nonlinear equations in both the equality and inequality constraints of the optimization problem, the classical Sequential Quadratic Programming (SQP) algorithm [29] is used as an example in this paper. The final coordinated control scheme can be obtained through the optimization solution method.
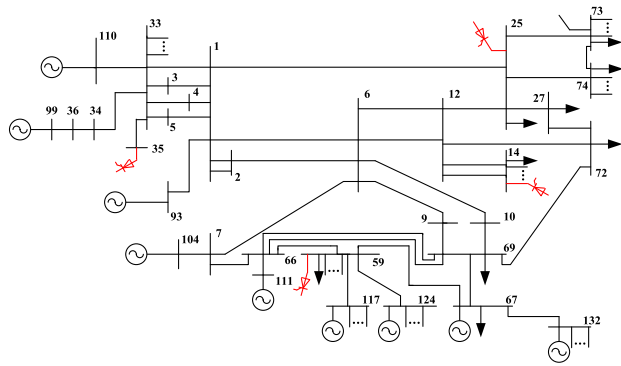
FIGURE 3. The modified IEEE50-generator system.

FIGURE 4. The frequency dynamic curve of different methods.

V. SIMULATION ANALYSIS

A. SIMULATION SYSTEM

In this paper, the IEEE 50-generator system is improved and 4 HVDC links are added. The improved multi-HVDC asynchronous power grid is shown in Fig. 3. This system mainly includes 50 generators, 90 load buses and 4 DC buses. It is set that the load type in the system is composed of constant power and constant impedance, and their proportions are 94.98% and 5.02% respectively.

The improved IEEE 50-generator system has 4 HVDC links interconnected with other power grids, which are linked to node 14, 25, 35 and 59 respectively. For convenience of distinction, they will be referred to as Link1, 2, 3 and 4 in the following introduction. Link1 and Link2 are used for power sending, and Link3 and Link4 are used for power receiving. Their main parameters are listed in Table 1 below.

TABLE 1. The main parameters of the simulation case.

Parameters	Link1	Link2	Link3	Link4
P_{dc0} / (MW)	1000	1200	1500	1200
ΔP_{dcmin} / (MW)	-100	-120	-750	-600
ΔP_{dcmax} / (MW)	500	600	150	120
V_u / (kV)	800	1000	1000	1000
R_{dc} / (Ω)	1	1.5	1.5	1
D_I	1000	1400	1200	1200
$\Delta \omega_{sI}$ / (Hz)	0.2	0.2	0.2	0.2

In this section, the modified power system is simulated in PSS/E platform. The post-disturbance instantaneous data of the PSS/E simulation is used as the WAMS data. We set the simulation working condition of the system as follows: when $t = 5$s, the Line 1-25 is disconnected due to permanent three-phase short circuit fault, when $t = 5.08$s, the Generator 93 is removed due to the line fault, and we set the total simulation time of the system as 60s.

B. CASE ANALYSIS

1) CASE 1: ACCURACY COMPARISON OF THE FREQUENCY DYNAMIC ANALYSIS METHOD

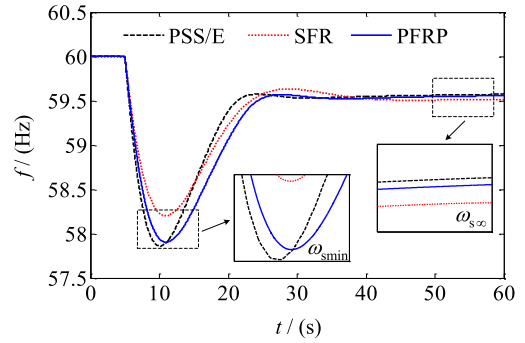The traditional methods of frequency response analysis are mostly based on single-generator equivalent model, such as the SFR model proposed in [30]. For convenience of expression, the frequency response analysis model proposed in this paper is denoted as PFRP model. We first get the real frequency dynamic curve of the system after disturbance through PSS/E according to the simulation working condition. Then, the data before and after disturbance obtained in PSS/E are taken as the WAMS data, and SFR model and PFRP model are respectively used to predict the frequency response curve after disturbance. Finally, the three curves are compared in Fig. 4. Furthermore, the lowest value, steady-state value and time corresponding to the lowest frequency point of the three curves are compared in Table 2.

TABLE 2. The comparison of prediction results of different methods.

Frequency	PSS/E	SFR		PFRP	
		Prediction	Error	Prediction	Error
ω_{smin} (Hz)	57.862	58.201	0.339	57.906	0.044
$\omega_{s\infty}$ (Hz)	59.574	59.517	0.057	59.563	0.011
t_{Fmin} (s)	10.274	10.951	0.677	10.982	0.031

As can be seen from Fig. 3 and Table 2, compared with SFR model, the frequency curve predicted by PFRP model is closer to the simulation results of PSS/E, especially for the lowest frequency. This result shows that the SFR model is usually only suitable for the estimation of steady frequency, and the estimation error of the lowest frequency is too large, which also makes it not conducive to the lowest frequency control. In contrast, the accuracy of PFRP model is quite high, which can lay a good foundation for the lowest frequency control.

2) CASE 2: EFFECTIVENESS VERIFICATION OF FREQUENCY COORDINATED CONTROL

The security level of the lowest frequency is set as $\omega_{\text{smin}} = 59$Hz. According to the case conditions, the post-disturbance lowest frequency obtained by PSS/E simulation is 57.862Hz, which is obviously below the security level. So the proposed coordinated control is activated at $t = 5.1$s.

Setting the control target of the lowest frequency is $\omega_{\text{set}} = 59$Hz, so the optimal EDCPS of each HVDC link can be
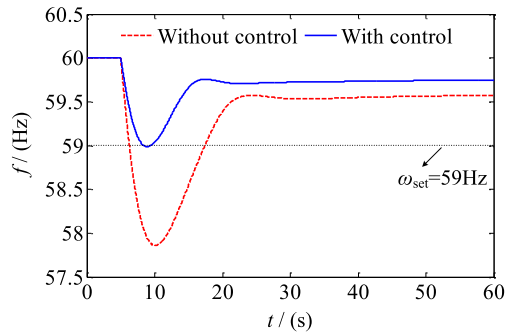
FIGURE 5. The frequency dynamic curves with and without the proposed control.

FIGURE 6. Frequency dynamic curves after the implementation of different control schemes.

obtained through the proposed frequency control method. The results are shown in Table 3.

TABLE 3. The optimal EDCPS amount of each HVDC link.

EDCPS	Link1	Link2	Link3	Link4
ΔP_{dc} (MW)	257.45	423.42	150	16.68

According to the control strategy shown in Table 3, the comparison of frequency curve with and without the proposed control can be obtained by PSS/E.

The key features of the post-control frequency curve in Fig. 5 are compared with the control target, and the results are shown in Table 4.

TABLE 4. Control accuracy analysis of the lowest frequency.

Description	Control target	Proposed control	Absolute error	Relative error(%)
ω_{smin} (Hz)	59.000	58.977	0.023	0.039
t_{Fmin} (s)	8.382	8.941	0.559	6.669

It can be seen from Fig. 5 and table 4 that after the implementation of the control strategy formulated in this paper, the lowest frequency after grid disturbance has been significantly increased and can be restored to the vicinity of the control target value, which verifies the effectiveness of the proposed control. In addition, it can be seen from the error statistics in Table 4 that the lowest frequency control error is about 0.02HZ and the lowest frequency arrival time error is about 0.5s after the control is implemented, which very specifically illustrates the accuracy of the proposed method in this paper.

3) CASE 3: IMPORTANCE AND NECESSITY VERIFICATION FOR THE OPTIMIZATION MODEL CONSTRAINTS

Three key constraints are considered in the proposed optimization model, including line transmission power constraint, node voltage security constraint and frequency deviation constraint. For convenience of description, they are denoted as LTPLC, NVSC and FDC in turn, and all constraints considered are denoted as AC. In order to verify the importance and necessity of these constraints for frequency
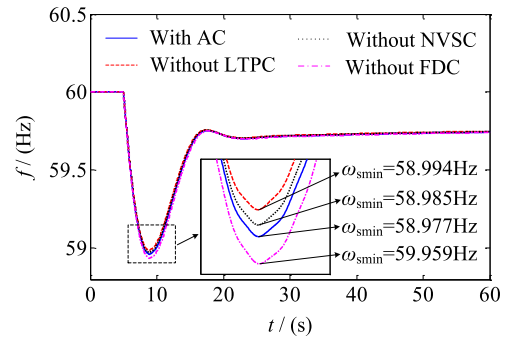
coordination control, this section makes control schemes without relevant constraints, and makes in-depth comparison of their control effects. By solving the corresponding optimization model, the control schemes under different conditions are shown in Table 5, and the corresponding control effects obtained by PSS/E are shown in Fig. 6.

TABLE 5. The frequency control schemes under different constraints.

Description	ΔP_{dc1} (MW)	ΔP_{dc2} (MW)	ΔP_{dc3} (MW)	ΔP_{dc4} (MW)
Without LTPC	0	575.62	150	101.22
Without NVSC	497.53	126.78	110.77	120
Without FDC	500	239.21	0	102.94

It can be seen from Table 5 and Fig. 6 that the EDCPS obtained under different constraints are obviously different, but both of them can improve the lowest frequency accurately to the target value, and the frequency dynamic curves are basically consistent.

Therefore, in order to verify the importance of the constraints considered, the relevant electrical quantities are compared under different control schemes. Firstly, for some heavy load lines in the power system, the power transmission of these lines after the control scheme completed with or without LTPC is counted, and the results are compared and analyzed in Table 6.

From Table 6, it is obvious that the control scheme with AC can ensure that the transmission power of all heavy load lines is within the limited range, while for the control scheme without LTPC, line 55~56, 55~58, 55~59, 55~61, 61~63 and 83~85 are overloaded. Thus, Table 6 fully illustrates the importance of considering LTPC.

Then, after implementing the control scheme with or without NVSC, the voltages of all nodes in the power grid are counted, and the results are shown in Fig. 7.

From the comparison of Fig. 7 (a) and (b), it can be seen that the voltage of some nodes, such as node 70, 138 and 139, exceed the security margin under the control scheme without NVSC, which verifies the necessity of considering NVSC.

Finally, with or without FDC control scheme, the frequency deviation comparison of opposite-end power

TABLE 6. Statistics, analysis and comparison of line transmission power.

| Line no.	P_{Tmax} (MW)	With AC		Without TPLC	
		P_T (MW)	$P_{Tmargin}$ (MW)	P_T (MW)	$P_{Tmargin}$ (MW)
55~56	201	197.0027	3.9973	207.3808	-6.3808
55~58	180	177.8472	2.1528	209.2363	-29.2363
55~59	180	179.3347	0.6653	200.2974	-20.2974
55~61	151	151	0	183.4004	-32.4004
61~62	127	119.5732	7.4268	126.7011	0.2989
61~63	124	117.3737	6.6263	128.7131	-4.7131
61~74	104	88.0122	15.9878	93.0917	10.9083
61~119	124	113.1113	10.8887	120.9289	3.0711
82~83	152	146.794	5.206	149.3164	2.6836
82~84	150	143.3879	6.6121	145.7921	4.2079
82~86	149	143.3634	5.6366	145.8306	3.1694
82~87	150	145.0608	4.9392	147.3035	2.6965
82~88	149	144.0185	4.9815	146.2402	2.7598
82~89	149	144.5325	4.4675	146.5951	2.4049
82~98	148	142.9386	5.0614	145.3748	2.6252
82~99	148	144.0293	3.9707	146.4861	1.5139
83~85	116	114.4943	1.5057	117.8791	-1.8791
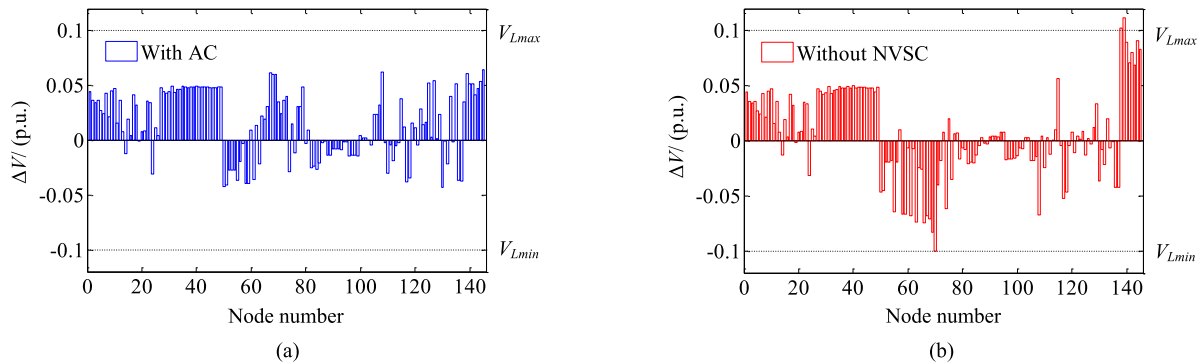
FIGURE 7. The deviations of the node voltage. (a) After implementing the control scheme with AC. (b) After implementing the control scheme without NVSC.

grids obtained through PSS/E verification is shown in Table 7 below.

TABLE 7. The multi-HVDC opposite-end grids frequency variation.

Description	$\Delta\omega_{sl1}$ (Hz)	$\Delta\omega_{sl2}$ (Hz)	$\Delta\omega_{sl3}$ (Hz)	$\Delta\omega_{sl4}$ (Hz)
With AC	0.188	0.113	0.047	0.077
Without FDC	0.213	0.057	0	0.158

It can be seen from Table 7 that when the FDS is not taken into account, with the change of the transmission power of Link1, the frequency variation of the first interconnected power grid is serious, resulting in a new problem of frequency stability.

VI. CONCLUSION
In this paper, with regard to the multiple HVDC asynchronous power system, a frequency dynamic analysis model is proposed by using the post-disturbance WAMS data. For the problem of the lowest frequency below the security level, this paper takes advantage of the EDCPS of multiple HVDC links to propose an optimal frequency control strategy. It can not only improve the recovery of the lowest frequency to the target value after disturbance, but also ensure the node voltage level, power flow of AC lines, and the frequency variation of multi-HVDC opposite-end grids keep in the security state after the control implemented. Through multiple case analysis, the accuracy and superiority of the frequency dynamic analysis model and the advanced performance of the coordinated control have been proved.

REFERENCES
[1] M. Wang, T. An, H. Ergun, Y. L. Lan, B. Anderson, M. Szechtman, W. Leterme, J. Beerten, and D. V. Hertem, "Review and outlook of HVDC grids as backbone of transmission system," *CSEE J. Power Energy Syst.*, vol. 7, no. 4, pp. 797–810, Jul. 2021.

[2] S. Gao, Q. Liu, and G.-B. Song, "Current differential protection principle of HVDC transmission system," *IET Gener., Transmiss. Distrib.*, vol. 11, no. 5, pp. 1286–1292, Jan. 2017.

[3] J. Wang, M. Huang, C. Fu, H. Li, S. Xu, and X. Li, "A new recovery strategy of HVDC system during AC faults," *IEEE Trans. Power Del.*, vol. 34, no. 2, pp. 486–495, Jan. 2019.

[4] M. A. Elizondo, N. Mohan, J. O'Brien, Q. H. Huang, D. Orser, W. Hess, H. Brown, W. C. Zhu, D. Chandrashekhara, Y. V. Makarov, D. Osborn, J. Feltes, H. Kirkham, D. Duebner, and Z. Y. Huang, "HVDC macrogrid modeling for power-flow and transient stability studies in North American continental-level interconnections," *CSEE J. Power Energy Syst.*, vol. 3, no. 4, pp. 390–398, Dec. 2017.

[5] H. Rao, W. Wu, T. Mao, B. Zhou, C. Hong, Y. Liu, and X. Wu, "Frequency control at the power sending side for HVDC asynchronous interconnections between Yunnan power grid and the rest of CSG," *CSEE J. Power Energy Syst.*, vol. 7, no. 1, pp. 105–113, Jul. 2020.

[6] Y. Hu, S. Xue, H. Zhang, H. Zhang, X. X. Feng, C. H. Tang, Y. Li, and P. Zheng, "Cause analysis and enlightenment of global blackouts in the past 30 years," (in Chinese), *Electr. Power*, vol. 54, no. 10, pp. 204–210, Oct. 2021.

[7] S. Abdelwahid, A. Babiker, A. Eltom, and G. Kobet, "Hardware implementation of an automatic adaptive centralized underfrequency load shedding scheme," *IEEE Trans. Power Del.*, vol. 29, no. 6, pp. 2664–2673, Dec. 2014.

[8] U. Rudez and R. Mihalic, "WAMS-based underfrequency load shedding with short-term frequency prediction," *IEEE Trans. Power Del.*, vol. 31, no. 4, pp. 1912–1920, Aug. 2016.

[9] Y. Zuo, G. Frigo, A. Derviškadic, and M. Paolone, "Impact of synchrophasor estimation algorithms in ROCOF-based under-frequency load-shedding," *IEEE Trans. Power Syst.*, vol. 35, no. 2, pp. 1305–1316, Mar. 2020.

[10] Z. Hu, S. Liu, W. Luo, and L. Wu, "Resilient distributed fuzzy load frequency regulation for power systems under cross-layer random Denial-of-Service attacks," *IEEE Trans. Cybern.*, vol. 52, no. 4, pp. 2396–2406, Apr. 2022.

[11] G. Liu, J. H. Park, C. Hua, and Y. Li, "Hybrid dynamic event-triggered load frequency control for power systems with unreliable transmission networks," *IEEE Trans. Cybern.*, early access, Apr. 12, 2022, doi: 10.1109/TCYB.2022.3163271.

[12] P. Kou, D. Liang, Z. Wu, Q. Ze, and L. Gao, "Frequency support from a DC-grid offshore wind farm connected through an HVDC link: A communication-free approach," *IEEE Trans. Energy Convers.*, vol. 33, no. 3, pp. 1297–1310, Sep. 2018.

[13] I. M. Sanz, P. D. Judge, C. E. Spallarossa, B. Chaudhuri, and T. C. Green, "Dynamic overload capability of VSC HVDC interconnections for frequency support," *IEEE Trans. Energy Convers.*, vol. 32, no. 4, pp. 1544–1553, Dec. 2017.

[14] M. M. Kabsha and Z. H. Rather, "A new control scheme for fast frequency support from HVDC connected offshore wind farm in low-inertia system," *IEEE Trans. Sustain. Energy*, vol. 11, no. 3, pp. 1829–1837, Jul. 2020.

[15] K. Q. Sun, H. Q. Xiao, S. Y. Liu, and Y. L. Liu, "Machine learning-based fast frequency response control for a VSC-HVDC system," *CSEE J. Power Energy Syst.*, vol. 7, no. 4, pp. 688–697, Jul. 2021.

[16] F. D. Bianchi, J. L. Dominguez-Garcia, and T. K. Vrana, "Distributed frequency control with partial information using MT-HVDC grids and WPPs," *IEEE Syst. J.*, vol. 13, no. 2, pp. 1694–1701, Jun. 2019.

[17] A. Bidadfar, O. Saborío-Romano, J. N. Sakamuri, N. A. Cutululis, V. Akhmatov, and P. E. Sørensen, "On feasibility of autonomous frequency-support provision from offshore HVDC grids," *IEEE Trans. Power Del.*, vol. 35, no. 6, pp. 2711–2721, Dec. 2020.

[18] T. N. Pham, H. Trinh, and A. M. T. Oo, "Distributed control of HVDC links for primary frequency control of time-delay power systems," *IEEE Trans. Power Syst.*, vol. 34, no. 2, pp. 1301–1314, Mar. 2019.

[19] Q. Zhang, J. D. McCalley, V. Ajjarapu, J. Renedo, M. A. Elizondo, A. Tbaileh, and N. Mohan, "Primary frequency support through North American continental HVDC interconnections with VSC-MTDC systems," *IEEE Trans. Power Syst.*, vol. 36, no. 1, pp. 806–817, Jan. 2021.

[20] H. Rao, W. Wu, T. Mao, B. Zhou, C. Hong, Y. Liu, and X. Wu, "Frequency control at the power sending side for HVDC asynchronous interconnections between Yunnan power grid and the rest of CSG," *CSEE J. Power Energy Syst.*, vol. 7, no. 1, pp. 105–113, Jan. 2021.

[21] M. N. Ambia, K. Meng, W. Xiao, A. Al-Durra, and Z. Y. Dong, "Adaptive droop control of multi-terminal HVDC network for frequency regulation and power sharing," *IEEE Trans. Power Syst.*, vol. 36, no. 1, pp. 566–578, Jan. 2021.

[22] Y. Liu, Y. Song, Z. Wang, and C. Shen, "Optimal emergency frequency control based on coordinated droop in multi-infeed hybrid AC-DC system," *IEEE Trans. Power Syst.*, vol. 36, no. 4, pp. 3305–3316, Jul. 2021.

[23] B. Ning, Q.-L. Han, and L. Ding, "Distributed finite-time secondary frequency and voltage control for islanded microgrids with communication delays and switching topologies," *IEEE Trans. Cybern.*, vol. 51, no. 8, pp. 3988–3999, Aug. 2021.

[24] L. Jin, Y. He, C.-K. Zhang, X.-C. Shangguan, L. Jiang, and M. Wu, "Robust delay-dependent load frequency control of wind power system based on a novel reconstructed model," *IEEE Trans. Cybern.*, vol. 52, no. 8, pp. 7825–7836, Aug. 2022.

[25] J. Yang, Q. Zhong, K. Shi, and S. Zhong, "Dynamic-memory event-triggered H_∞ load frequency control for reconstructed switched model of power systems under hybrid attacks," *IEEE Trans. Cybern.*, vol. 1, no. 1, pp. 1–13, May 2022.

[26] J. A. Laghari, H. Mokhlis, M. Karimi, A. H. AbuBakar, and H. Mohamad, "A new under-frequency load shedding technique based on combination of fixed and random priority of loads for smart grid applications," *IEEE Trans. Power Syst.*, vol. 30, no. 5, pp. 2507–2515, Sep. 2015.

[27] T. T. Teo, T. Logenthiran, W. L. Woo, K. Abidi, T. John, N. S. Wade, D. M. Greenwood, C. Patsios, and P. C. Taylor, "Optimization of fuzzy energy-management system for grid-connected microgrid using NSGA-II," *IEEE Trans. Cybern.*, vol. 51, no. 11, pp. 5375–5386, Nov. 2021.

[28] A. Wang, W. Liu, T. Dong, X. Liao, and T. Huang, "DisEHPPC: Enabling heterogeneous privacy-preserving consensus-based scheme for economic dispatch in smart grids," *IEEE Trans. Cybern.*, vol. 52, no. 6, pp. 5124–5135, Jun. 2022.

[29] M. S. P. Subathra, S. E. Selvan, T. A. A. Victoire, A. H. Christinal, and U. Amato, "A hybrid with cross-entropy method and sequential quadratic programming to solve economic load dispatch problem," *IEEE Syst. J.*, vol. 9, no. 3, pp. 1031–1044, Sep. 2015.

[30] H. Ye, W. Pei, L. Kong, and T. An, "Low-order response modeling for wind farm-MTDC participating in primary frequency controls," *IEEE Trans. Power Syst.*, vol. 34, no. 2, pp. 942–952, Mar. 2019.

YI HU was born in Chengdu, China, in 1990. He received the Ph.D. degree from the College of Electrical Engineering, Southwest Jiaotong University (SWJTU), China, in 2019. He has been a Lecturer with the School of Electrical Engineering and Electronic Information, Xihua University, since 2020. His research interests include power system frequency stability analysis and control, especially for the AC/DC hybrid power grid.

XIA LEI (Member, IEEE) received the Ph.D. degree in electrical engineering from Sichuan University. She is currently a Professor with the School of Electrical Engineering and Electronic Information, Xihua University. Her research interests include the optimal operation of electrical systems with renewable energy and power markets.

TAO HUANG (Member, IEEE) received the Ph.D. degree from the Polytechnic University of Turin, Turin, Italy, where he is currently pursuing the Ph.D. degree with the Department of Energy. His research interests include critical infrastructure protection, vulnerability detection and resilience enhancement, electricity markets, and smart grids.

YU ZHANG received the B.E. and M.E. degrees from Lanzhou Jiaotong University, China, in 2013 and 2016, respectively. He is currently pursuing the Ph.D. degree with the College of Electrical Engineering, Southwest Jiaotong University (SWJTU), China. His research interest includes the stability of power system with renewable energy.

● ● ●